Emerging Science Innovation, vol. 6, 2026, pp. 09-20

Analysis and Selection of the Best Global Geopotential Model for Lebanon

Mohamed Issa[1,*], Mohammad Abboud[2]

[1]Department of Surveying Engineering, LIU, IU Universities, Beirut, Lebanon,

[2]Department of Surveying Engineering, LIU University, Beirut, Lebanon

Received 01 August 2025; received in revised form 03 November 2025; accepted 04 November 2025

DOI: https://doi.org/10.46604/emsi.2026.15489

Abstract

Accurate transformation of Global Positioning System (GPS) derived ellipsoidal heights to orthometric heights necessitates the selection of an optimal Global Geopotential Model (GGM). This study aims to identify the most accurate freely available high-resolution GGM for Lebanon. The performance of five GMs, Earth Gravitational Model 2008 (EGM2008), SGG_UGM_1, SGG_UGM_2, GECO, and XGM2019e, is assessed. Geoidal undulation values are extracted for 28 geodetic benchmarks in the Rashaya district using a Geographic Information System and compared with reference data from the Lebanese Directorate of Geodetic Affairs. Vertical accuracy is quantified using the mean deviation (ΔN), standard deviation, and root mean square error (RMSE) between GGM-derived and reference heights. The analysis reveals that XGM2019e provides the highest accuracy, with the smallest mean deviation (ΔN = –0.25 m) and the lowest RMSE (±1.09 m). These results establish XGM2019e as the optimal GGM for Lebanon, ensuring precise height transformation and supporting advanced geodetic and geospatial analyses.

Keywords: Analysis, Geoidal Global Models, Orthometric Heights, GIS

1. Introduction

The advent of the Global Positioning System (GPS) has significantly transformed surveying practices, enabling faster and more precise data acquisition. One of its major applications is the determination of point elevations above the geoid, typically approximated by Mean Sea Level (MSL). However, GPS intrinsically provides ellipsoidal heights relative to the World Geodetic System 1984 (WGS84) reference ellipsoid [1], whereas most engineering and geodetic applications require orthometric heights referenced to the geoid. This discrepancy arises from the separation between the ellipsoid and the geoid, known as geoid undulation (*N*). Therefore, converting GPS-derived ellipsoidal heights into orthometric heights necessitates the use of a suitable Global Geopotential Model (GGM) or a precise Digital Elevation Model (DEM). Fig. 1 represents the relation between the ellipsoidal height (*h*) and the orthometric height (*H*) [2] and the geoidal undulation for the point (*N*). Thus, it can be expressed as:

$$h = H + N \tag{1}$$

Historically, geoid undulation was computed using Stokes' integral [3]. In recent decades, the Earth Gravitational Model 2008 (EGM2008) has been widely used for height conversion. EGM2008 has demonstrated satisfactory accuracy for various geodetic applications, as confirmed in numerous studies [4, 5]. Nevertheless, GGMs mainly capture the long-wavelength components of the Earth's gravity field, and several methods, such as Stokes' formula [6], least squares collocation, and polynomial fitting [7], have been proposed to improve their performance. In countries lacking national geoid models, GGMs remain essential for deriving geoid heights and gravity anomalies via spherical harmonic analysis [8]. This was the main reason

* Correspondence author: Mohamed.issa@liu.edu.lb; +961-71031299

that prompted national agencies, such as the International Center for Global Earth Models (ICGEM), to develop new and modern GGMs based on contemporary data gathering techniques, including Light Detection and Ranging (LIDAR), Gravity field and steady-state Ocean Circulation Explorer (GOCE) satellites, and Gravity Recovery and Climate Experiment (GRACE) [9].

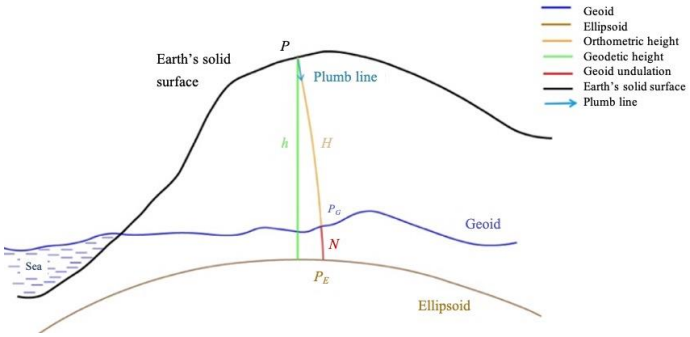

Fig. 1 Relation between ellipsoidal height, orthometric height, and geoidal undulations

The Gravity field and steady-state Ocean Circulation Explorer (GOCE) mission (2009-2013) provided geoid measurements with an accuracy of 1-2 cm at a 100 km resolution, while the Gravity Recovery And Climate Experiment (GRACE) has yielded over a decade of high-quality gravity data. Successive releases of GOCE-only, GRACE-only, and combined GGMs—such as SGG_UGM_2 and XGM2019e—have improved Earth's gravity field modeling. Evaluating these models is crucial for assessing their accuracy and potential benefits for regional geoid determination, particularly since Lebanon has officially adopted the EGM2008 model.

On a global scale, comparative studies, such as those conducted in Egypt [10], have demonstrated that modern GGMs (e.g., GECO and EIGEN-6C4) can outperform older models in representing regional gravity fields. However, no comprehensive assessment has been conducted for Lebanon using recent high-resolution GGMs. This gap hinders the selection of an optimal model for height transformation and geodetic applications in the country.

The present study addresses this gap by evaluating the performance of five modern, freely available GGMs—EGM2008, SGG_UGM_1, SGG_UGM_2, GECO, and XGM2019e—over Lebanon. Geoidal undulations from each model are compared with precise GPS/levelling data from 28 benchmarks in the Rashaya district, enabling a statistical assessment of their accuracy.

The remainder of this paper is structured as follows: Section 2 describes the tested GGMs dataset, Section 3 presents the study area, the available data, and the downloaded data, Section 4 illustrates the adopted methodology, Section 5 reports and discusses the results, Section 6 statistically tests the Hypothesis of the problem, and finally Section 7 provides conclusions and recommendations.

2. Tested Global Geopotential Models (GGMs)

In the current research, five GGM models have been selected to evaluate their accuracy using GPS/levelling points and to identify the most accurate one to be used in Lebanon for topographic mapping and other surveying applications. These GGM models are available on the website of the International Center for Global Earth Models, ICGEM [11]. The selection criteria were primarily based on the maximum degree and order of each GGM, with particular consideration given to models developed over the past two decades. Since EGM2008 is currently the most frequently used gravity field model, and is constructed with possibly the best global $5' \times 5'$ data set of gravity anomaly data from terrestrial observations, satellite altimetry, and fill-in gravity anomalies from RTM forward modelling and the GRACE normal equation (NEQ) of the Institute of Geodesy and Geoinformation of the University of Bonn (ITG)-GRACE03S satellite-only model, the analyzed models are EGM2008 and any recent model that came after it and uses the same data used by the EGM2008 and add new additional data in its processing strategy. Those models are:

(1) EGM2008: The Earth Gravitational Model has been publicly released by the USA National Geospatial-Intelligence Agency (NGA) EGM development team. It was developed in 2008 based on satellite tracking data, terrestrial gravity data, and altimetry data. This gravitational model is complete to the spherical harmonic degree and order 2159 [12], and it contains additional coefficients extending to degree 2190 and order 2159.

(2) GECO: The European Space Agency's (ESA) dedicated satellite gravity field mission, the Gravity Field and Steady-state Ocean Circulation Explorer (GOCE), is planned to achieve a 1-2 cm accuracy level for geoid undulation and at 1-2 mGal level for gravity anomalies down to a spatial resolution of 100 km. GECO is a global gravity model, computed by combining the GOCE-only TIMR5 (time-wise approach) solution with EGM2008 [13]. From degree 360 to degree 2190, the GECO coefficients are the same as EGM2008.

(3) SGG-UGM-1 is complete to degree and order 2159, and is derived using the proposed calculation strategies developed by the German GFZ research center. The fully occupied normal equation system up to degree and order 220, formed by GOCE satellite data, and the block-diagonal normal equation system up to degree and order 2159, formed by EGM2008 gravity anomaly data, are used for the combination [14].

(4) SGG-UGM-2 differs from SGG-UGM-1 in three main aspects: the use of ellipsoidal harmonic functions, the update of gravity anomaly data in marine areas, and the employment of the GRACE NEQ. It combines altimetry data, satellite gravity data, and surface gravity anomalies to compute the high-resolution gravity field model SGG-UGM-2 up to degree and order 2160 [15].

(5) XGM2019e_2159 is a combined global gravity field model represented by spheroidal harmonics up to degree and order (d/o) 5399, corresponding to a spatial resolution of 2′ (~ 4 km). XGM2019e is composed of three main data sources: the combined satellite-only model GOCO06s (where GOCO06s is a combined satellite-only model consisting mainly of data from the GOCE TIM6, [16] and GRACE [17] missions), the 15′ ground gravity anomaly dataset provided by NGA, and the 1′ min augmentation dataset consisting of gravity anomalies derived from altimetry over the oceans and topography over the continents [18].

Table 1 summarizes the main characteristics of those GGM models, from which it can be observed that the selection of such models depicts a variety in nature in terms of development year, maximum model degree, and the types of data utilized in each model's development. In Table 1, S is for satellite (e.g., GRACE, GOCE, and Laser Geodynamics Satellite (LAGEOS)), A is for altimetry, G is for ground data (e.g., terrestrial, shipborne, and airborne measurements), and T is for Topography.

Table 1 Characteristics of the tested released high-resolution gravity field models

Model name	Year	Max degree	Input Data	Reference
EGM2008	2008	2159 (full), extended to 2190	A, G, S(GRACE)	[19]
XGM2019e_2159	2019	2159 (ICGEM usable truncation)	A, G, S(GOCO05s), T	[18]
GECO	2015	2190	EGM2008, S(GOCE)	[13]
SGG-UGM-1	2018	2159	EGM2008, S(GOCE)	[20]
SGG-UGM-2	2020	2190	A, EGM2008, S(GOCE), S(GRACE)	[15]

3. Case Study and Available Data

To ground our methodological framework in a concrete, practical context, the analysis now applies the tested GGMs to a focused case study. Rashaya is selected for its distinct practical gradients and topographical variability, providing an ideal empirical setting to interpret the model's conditional dependencies.

3.1 The Rashaya study area

Rashaya Al Wadi and its variations constitute one of the cities of the Rashaya District in the Western Bekaa Governorate of Lebanon. It is at an approximate altitude of 1250 meters above sea level on the western slopes of Jabal Al-Sheikh, southeast of Beirut, near the Syrian border. The study area, as illustrated in Fig. 2, is part of the Rashaya District where its topographic land contains mountains and plains, and its area is approximately 118 km^2. The elevation of the study area ranges approximately from 960 m to 1460 m, and accordingly, the tested area has variable topography, approximately 11.5 Km x 9.2 Km with a study area of approximately 106 Km^2.

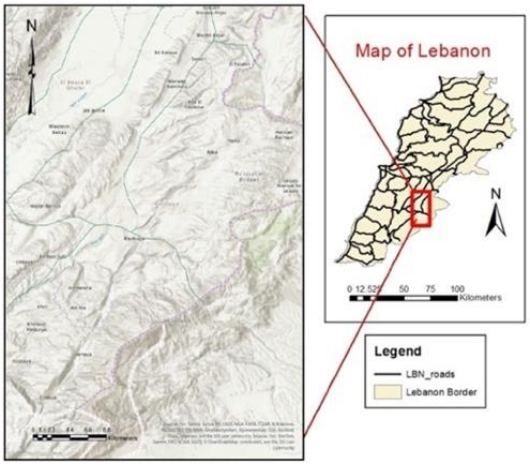

Fig. 2 Google Earth topographic surface of the Rashaya study area [21]

3.2 Available data

There are two types of available data. The first one is the downloaded geoidal models that will be tested for suitability, and the second is the known ground control points that will serve as a reference for comparison.

3.2.1 Geoidal GGM models

The available tested GGM models for the study area were downloaded from the Earth Data USGS site [22] and the International Center for Global Earth Models (ICGEM) site [11], based on the study area's boundary coordinates, type, source, and resolution. As an example of the downloaded data, the EGM2008 geoid height model for Lebanon, including the study area (Rashaya region), is shown in Fig. 3. From this Figure, when extracting the geoidal undulation values for Lebanon only, it can be noticed that the geoidal undulation values range 7.169 m and vary from 21.574 m to 28.743 m, with a mean value of 26.087 m.

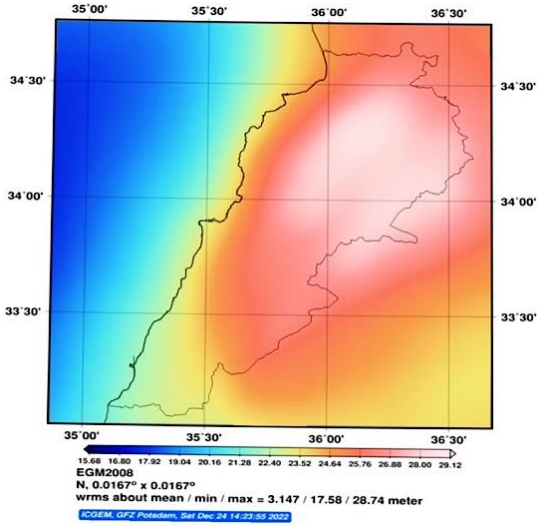

Fig. 3 EGM2008 geoid height model for Lebanon, including the Rashaya region

Table 2 Statistical values for the GGM models tested in Lebanon (m units)

GGM	EGM2008	SGG-UGM-1	SGG-UGM-2	GECO	XGM2019e_2159
Minimum	21.574	21.519	21.510	21.530	21.364
Maximum	28.743	28.824	28.872	28.758	28.767
Mean	26.087	26.136	26.170	26.114	26.139
Range	7.169	7.305	7.362	7.228	7.403
Standard Deviation	1.724	1.763	1.777	1.749	1.733

Concerning the other downloaded tested GGMs (SGG-UGM-1, SGG-UGM-2, GECO, and XGM2019e_2159), Table 2 summarizes the statistical values of the geoidal undulation values obtained from these models.

Table 2 shows that the differences among the tested models, whether in mean values or standard deviation values, were very close to each other and at the centimeter level. This can be seen in Fig. 4. In addition, it can be observed that the newer the GGM model version and the more data included in its calculation, the wider the range of geoidal values for the tested area in Lebanon and the smaller the standard deviation of the corresponding model.

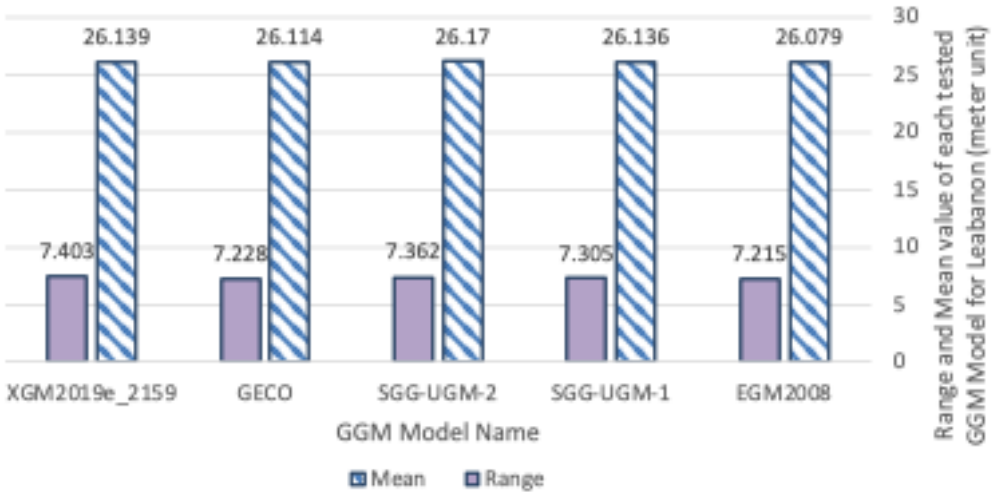

Fig. 4 Average and range statistical values of the GGM models tested for Lebanon

3.2.2 Topographic and cadastral maps

One topographic map sheet at a scale of 1:20,000 covering the Rashaya study site was selected to be used as a reference to analyze the tested GGMs. The map has been prepared photographically by the Geographic Affairs Authority GAA from aerial orthophotography taken in 2015 with a resolution of 0.5 m. The map is based on the Clarck 1880 ellipsoid with oblique stereographic projection. In addition, six cadastral maps for the Rashaya District, which illustrate the distribution of available GCPs, were obtained.

3.2.3 Known control points

The available Global Geoidal Models GGMs are assessed using 28 known GPS/Levelling Ground Control Points GCP stations with known ellipsoidal and orthometric heights. The distribution of these stations is shown in Fig. 5. From this figure, it can be observed that the checkpoints are distributed approximately throughout the entire 11.5 x 9.2 square km study area. The GCP stations were obtained from the Geographic Affairs Authority GAA and based on the Clarck 1880 ellipsoid with oblique stereographic projection [23].

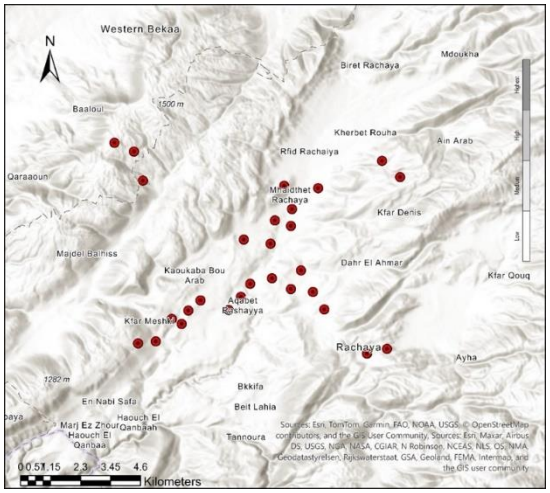

Fig. 5 Illustration of the check GCPs distribution throughout the Rashaya study area

4. Methodology

Using the downloaded GGM models and the known GCPs, the adopted procedures for analyzing the best GGM for the study area are depicted in Figure 6:

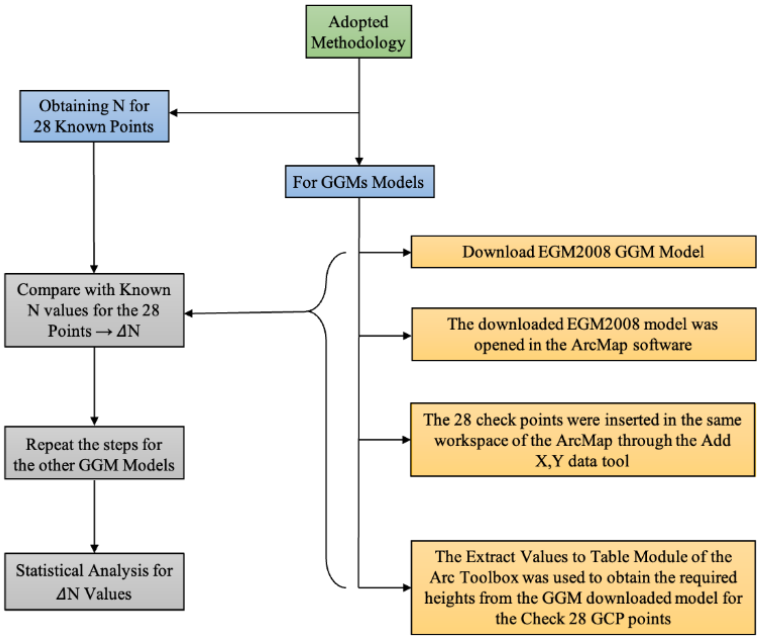

Fig. 6 Diagram illustrating the adopted methodology for testing the best GGM model

5. Results and Discussion

Initially, as illustrated in the previous figure (Fig. 6), the geoidal undulation values for each of the 28 checkpoints were extracted from each global GGM model using ArcMap software. Afterwards, the 28 extracted values were compared to the known values, and the resulting residuals were listed in the Excel software. The statistical indicators and Probability Distribution Function PDF graph were also calculated and drawn using Excel and the Statistica software for the evaluated residuals.

Table 3 shows the statistics of the residuals (discrepancies between the geoid heights from the global model and the effective ones of the known GPS stations). From this, it can be observed that the best performance is provided by the XGM2019e_2159 model (Average = -0.253 m and RMS = 1.094 m), while the worst was related to the EGM2008 model (Average = -0.458 m and RMS = 1.160 m).

Table 3 Statistics of the residuals between the geoidal heights of the GNSS 28 check stations and those supplied by each global GGM model (units in meters)

Parameter	ΔN from EGM2008	ΔN from SGG_UGM_1	ΔN from SGG_UGM_2	ΔN from GECO	ΔN from XGM2019e_2159
Average	-0.458	-0.394	-0.434	-0.376	-0.253
Min	-3.326	-3.259	-3.297	-3.238	-3.069
max	2.647	2.703	2.659	2.715	2.803
S.D.	1.085	1.085	1.085	1.085	1.084
RMSE	1.160	1.136	1.150	1.094	1.094

Additionally, for better interpretation, the statistics are illustrated in Fig. 7. From this graph, the same conclusion about the best and worst GGM models can be easily derived, that is, the best performance is provided by the XGM2019e_2159 model, which has the smallest average of the calculated differences and the least RMSE and standard deviation values.

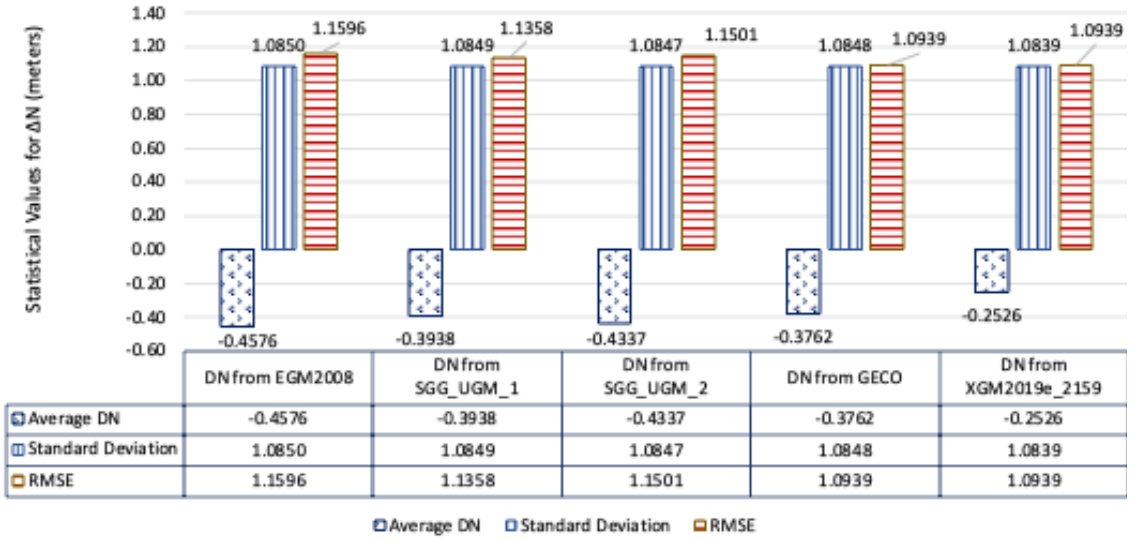

Fig. 7 Statistics for the geoidal height differences between known and derived GGM values at the 28 check stations

6. Hypothesis of the Problem

A hypothesis is a proposed statement about the characteristics of a population distribution. Hypothesis testing is a formal procedure that uses sample data to decide whether to support or reject the proposed statement, commonly referred to as the null hypothesis [24]. Typically, a test statistic is calculated from the observed sample data based on the assumptions of the null hypothesis. The test statistic value is then compared to a predefined critical region. The null hypothesis is rejected if the test statistic falls within the critical region; otherwise, it is not rejected.

However, the null hypothesis is that the differences have a normal distribution with mean φ and variance σ^2. The sample mean ΔN_{mean} and sample variance S^2 were tested to determine whether they belong to a normal distribution N (φ, σ^2). For statistical testing, the assumption is that the population mean, φ, and variance σ^2, are normally distributed. Thus, to test if the sample mean ΔN_{mean} and variance S^2 are within the confidence interval (CI) of the population mean, φ, and variance σ^2 from which the sample is drawn, the following hypothetical statistical tests were used:

Let n_j be the geoid undulation differences from the recent geoid models, such that: (n_j =1, 2, 3, …) with estimated statistics ΔN_{mean}, and S^2. Then, the sample mean N_{mean} has a T-distribution function that can be computed by [12], [28]:

$$\frac{\Delta N_{mean} - \phi}{\frac{S}{\sqrt{n}}} = t_{n-1} \quad (2)$$

where (n-1) is the degree of freedom, the equal sign (=) indicates that the right-hand side is distributed with respect to the left-hand side. If the null hypothesis is true, $T_{\text{N-1}}$ follows a *t* distribution with $n - 1$ degrees of freedom. If ΔN_{MEAN} and S are the mean and standard deviation of a random sample from a normal distribution with unknown variance σ^2, a $100(1 - \alpha)\%$ CI on ϕ is given by:

$$\Delta N - t_{0.95}^{(n-1)} \times \frac{S}{\sqrt{n}} \leq \phi \leq \Delta N + t_{0.95}^{(n-1)} \times \frac{S}{\sqrt{n}} \quad (3)$$

These tests were performed to quantify whether the estimated population mean, φ, and variance S^2 lies within the CI constructed from the sample. The information used to validate the geoid models' truthfulness is presented in Table 3. The population means φ can be tested as follows:

Let the null hypothesis be Ho, where:

H_0: $\mu = 0$ (No significant bias: mean difference $\Delta N_{mean} = 0$)

H_1: $\mu \neq 0$ (Significant bias exists)

$$\varphi_{XGM\,2019e} = -0.253m \quad (4)$$

Substituting the sample statistics into Eq. (2), the test statistic is obtained as: $T_0 = \frac{|-0.253-0|}{\frac{1.0839}{\sqrt{28}}} = 1.234$. The critical t-value at $\alpha = 0.05$ (two-tailed) with df = 27 is 2.05183 [25]. Since the calculated t-value is less than the critical value, the null hypothesis cannot be rejected. Thus, the mean difference ($\Delta N = -0.253$ m) is not statistically significant at the 95% confidence level. Based on Eq. (3), the 95% confidence interval for the population mean φ is obtained as:

$$CI_{95\%} = [-0.6733, +0.1673]m \quad (5)$$

In addition, if the aim is to test whether the variance in differences of the 28 values in the test area (variance of the differences is 1.1748 m^2). To provide evidence to support the claim that the variation of the differences is less than the population variance $\sigma_o = 1$ at a 95 % confidence level, the following equation of the Chi-square test was applied [25], which can be represented as:

$$X_{\Delta N}^2 = (n-1) \times S^2 = \sigma_o^2 \times 31.7242 \quad (6)$$

For a two-sided $100(1 - \alpha)\%$, and using degrees of freedom $\nu = 27$, CI for the variance is: $\frac{(n-1)\times S^2}{\chi^2_{1-\alpha/2,\nu}}, \frac{(n-1)\times S^2}{\chi^2_{\alpha/2,\nu}}$, and from the Chi-square tables, it can be found that $\chi^2_{0.975,27} = 43.19451, \chi^2_{0.005,27} = 14.57338$, and accordingly, the standard deviation is located between the two limits $\sigma = 1.0839 \in (0.857001, 1.147542)m$. Where: n=28, the sample standard deviation $S = 1.0839$ m, and the sample variance $S^2 = 1.1749$ m^2. Therefore, with 95% confidence, the true standard deviation lies between approximately 0.857 m and 1.475 m, and provides statistical evidence that the sample variance is significantly less than the population variance, assuming that the underlying residuals are approximately normally distributed.

For example, to verify the randomly accepted residuals, Fig. 8 displays the distribution graph of the calculated residuals. This figure shows that the residuals distribution follows the bell-shaped curve, and no outliers exist for the five variables (tested geoidal models). Moreover, the mode or peak of each graph for the tested geoidal models shifted from the zero value by about -0.26 m, which is the same conclusion derived previously and recommended to be added as vertical translation.

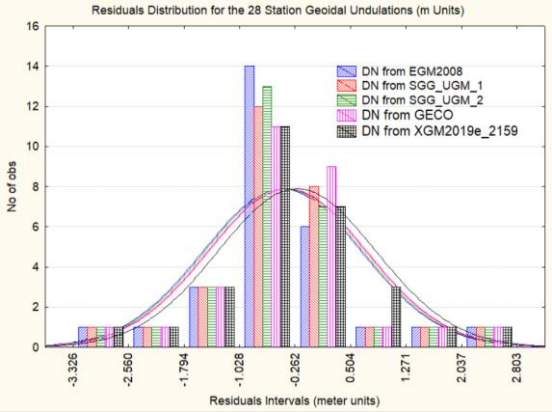

Fig. 8 Distribution of the calculated ΔN' residuals at the 28 check points for each GGM tested model

However, since the differences between different models are small, the normality test is not enough. Therefore, the following variance analysis of the ANOVA test was performed. This test is used when it is required to compare more than two models simultaneously. From Table 3, it can be seen that: K equals 5 groups, n = 28 points, and the total N= 140.

The overall grand mean:

$$\bar{X}_{ground} = \frac{\Sigma \chi}{K} = \frac{(-1.915)}{5} = -0.383 \tag{7}$$

The between-groups sum of squares:

$$SSB = n \times \Sigma\left(\chi_i - \bar{X}_{ground}\right)^2 = 0.70829 \tag{8}$$

Degrees of freedom for SSW equal to 140-5= 135, and:

$$SSW = pooled\ \text{var}iance \times (N-K) = \frac{\Sigma(n_j - 1) \times S_j^{\ 2}}{\Sigma(n_j - 1)} \times (N-K) = 158.867 \tag{9}$$

F-Statistic = 0.1505 is less than the F-Critical = 2.44, hence the one-way ANOVA results confirm the initial observation that the differences between the geoid models are minimal. The analysis found no statistically significant difference in the mean residuals between the five geoidal models.

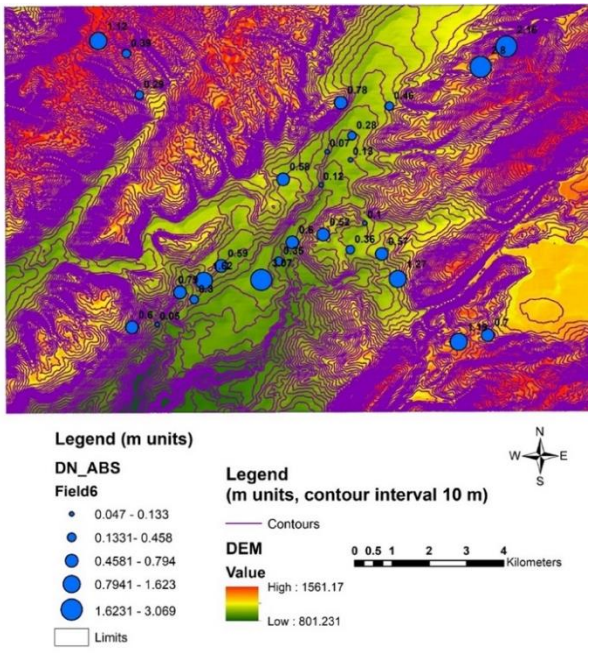

Fig. 9 Check points geoidal height differences from the XGM2019e_2159 model depicted above the Rashaya DEM

Since the model XGM2019e_2159 has the lowest RMSE, and since it is more recent and based on a broader set of input data, it is a more future-proof choice for future projects. The geoidal height differences between the known and the extracted values from the XGM2019e_2159 model were inserted as circles with variable radius (the radius varies according to the difference in geoidal height) above the Digital Elevation Model DEM of Rashaya and depicted in Fig. 9 for better analysis and because the tested area has variable topography.

The DEM is based on the Clarck 1880 Ellipsoid and obtained from the DEM files of SRTM that have been mosaiced into a seamless near-global coverage (up to 60 degrees north and south), and are available for download as 5-degree x 5-degree tiles, in the geographic coordinate system - WGS84 datum [26, 27].

These files are available for download in both Arc-Info American Standard Code for Information Interchange format (Arc-Info ASCII) format and as Georeferenced Tagged Image File Format (GeoTiff), for easy use in most GIS and Remote Sensing (RS) software applications. From Fig. 9, and as recognized also during the reconnaissance field survey, it can be noticed that the big differences are located in variable or rough topography locations, whereas the small differences are located in the nearly flat areas that have small variation in topography. This may be attributed to the fact that GGMs are typically derived from satellite observations and global gravity data, which are processed at a limited spatial resolution. Moreover, in rough terrain, where the elevation and gravity field change rapidly over short distances, GGMs tend to smooth out these variations due to their resolution limits.

7. Conclusions

The experiments carried out in this work confirm that the highest accuracy of XGM2019e_2159 compared to other new GGMs, i.e., EGM2008, SGG_UGM_1, SGG_UGM_2, and GECO. However, the findings also indicate that global geoid height models are often unsuitable for local applications. The main findings can be summarized as follows:

(1) The RMS calculated values (1.16 m for EGM2008, 1.136 m for SGG_UGM_1, 1.15 m for SGG_UGM_2, 1.094 m for GECO, and 1.094 m for XGM2019e_2159) resulting in the Rashaya region are inappropriate for accurate survey and representation but better results can be achieved if the XGM2019e_2159 is preventively adapted to the study area: for the Rashaya region, a vertical translation of the model is appropriate; in particular, 0.253 m should be subtracted from the original value of each undulation, where the new RMS equals 1.06 m instead of the old value of 1.09 m.

(2) Based on the current GNSS/leveling comparisons, the XGM2019e global geopotential model performs reliably over terrestrial regions. Notably, it exhibits a modest yet consistent improvement over previous models, particularly due to the incorporation of topographic information. Thus, it can be stated that XGM2019e performs more consistently on a global scale than other models. This seems reasonable because the topographic information used in XGM2019e is available globally with nearly constant quality, whereas the availability (and quality) of direct gravity field measurements is strongly location dependent.

This study represents ongoing research, and future work is planned to extend testing across the Lebanese territory. A larger dataset of reference points with known geoid undulation values will be employed, and separate analyses will be conducted over distinct terrain types, including flat, rugged, and moderately mountainous areas, to further investigate the potential for locally fitting a global geoid model. The better consistency and the fact that gravity field information provided by XGM2019e is globally available up to ~ 4 km can be important and expected to be valuable for applications such as consistent gravity field reduction in the frame of a compute–remove–restore process of regional gravity field modeling (especially in areas where the terrestrial data quality is low, or data access is restricted).

Conflicts of Interest

The authors declare no conflicts of interest regarding this manuscript.

References

[1] K. Pakoksung and M. Takagi, "Assessment and Comparison of Digital Elevation Model (DEM) Products in Varying Topographic, Land Cover Regions and Its Attributes: A Case Study in Shikoku Island," Japan," Model Earth Syst Environ, vol. 7, pp. 465-484, 2021.

[2] P. Maglione, C. Parente, and A. Vallario, "Accuracy of Global Geoid Height Models in Local Area: Tests on Campania Region (Italy)," International Journal of Civil Engineering and Technology, vol. 9, no. 3, pp. 1049-1057, 2018.

[3] A. Fanos, T. Rusul, S. Mohammed, and M. Suad, "Calculating of Adjusted Geoid Undulation Based on EGM08 and Mean Sea Level for Different Regions in Iraq," MATEC Web of Conferences, vol. 162, article no. 03028, 2018.

[4] W. A. Heiskanen and H. Moritz, "Physical Geodesy," Bulletin Géodésique, vol. 86, pp. 491-492, 1967.

[5] C. J. Nyoka, A. H. M. Din, M. F. Pa'suya, and A. H. Omar, "Rigorous Evaluation of Global Geopotential Models for Geoid Modelling: A Case Study in Kenya," Journal of African Earth Sciences, vol. 194, article no. 104612, 2022.

[6] K. M. A. Aziz, K. S. Rashwan, and N. Saba, "Evaluation of EGM96 and EGM08 Based on GPS/Levelling Heights in Egypt," South African Journal of Geomatics, vol. 12, no. 1, pp. 44-55, 2023.

[7] S. Lee, C. Choi, and J. Kim, "Evaluating the Suitability of the EGM2008 Geopotential Model for the Korean Peninsula Using Parallel Computing on a Diskless Cluster," Computers & Geosciences, vol. 52, pp. 132-145, 2013.

[8] D. S. Fazilova, A. Kazakov, and I. M. Alimukhamedov, "Improving Global Geoid by GPS and Leveling Data Over the Fergana Valley Territory," InterCarto. InterGIS, vol. 28, no. 1, pp. 568-579, 2022.

[9] B. Erol, "An Automated Height Transformation Using Precise Geoid Models," Scientific Research and Essays, vol. 6, no. 6, pp. 1351-1363, 2011.

[10] M. Rabah, A. El-Hattab, and M. Abdallah, "Assessment of the Most Recent Satellite Based Digital Elevation Models of Egypt," NRIAG journal of astronomy and geophysics, vol. 6, no. 2, pp. 326-335, 2017.

[11] ICGEM, "ICGEM International Center for Global Earth Models," http://icgem.gfz-potsdam.de/ICGEM/ICGEM.html, accessed in 2023.

[12] M. S. Peprah, Y. Y. Ziggah, and I. Yakubu, "Performance Evaluation of the Earth Gravitational Model 2008 (EGM2008)–a Case Study," South African Journal of Geomatics, vol. 6, no. 1, pp. 47-72, 2017.

[13] Q. Liu, M. Schmidt, L. Sánchez, L. Moisés, and D. Cortez, "High-Resolution Regional Gravity Field Modeling in Data-Challenging Regions for the Realization of Geopotential-Based Height Systems," Earth, Planets Space, vol. 76, no. 1, article no. 35, 2024.

[14] L. Wei, X. U. Xinyu, L. I. Jiancheng, and Z. H. U. Guangbin, "The Determination of an Ultra-High Gravity Field Model SGG-UGM-1 by Combining EGM2008 Gravity Anomaly and GOCE Observation Data," Acta Geodaetica et Cartographica Sinica, vol. 47, no. 4, article no. 425, 2018.

[15] W. Liang, J. Li, X. Xu, S. Zhang, and Y. Zhao, "A High-Resolution Earth's Gravity Field Model SGG-UGM-2 from GOCE, GRACE, Satellite Altimetry, and EGM2008," Engineering, vol. 6, no. 8, pp. 860-878, 2020.

[16] J. M. Brockmann, T. Schubert, T. Mayer-Gürr, and W. D. Schuh, "The Earth's Gravity Field as Seen by the GOCE Satellite: an Improved Sixth Release Derived with the Time-Wise Approach (GO_CONS_GCF_2_TIM_R6)," GFZ Data Services, 2019.

[17] A. Kvas, T. Mayer-Gürr, S. Krauß, J. M. Brockmann, T. Schubert, W. Schuh, et al., "The Satellite-Only Gravity Field Model GOCO06s," GFZ Data Services, 2019.

[18] P. Zingerle, R. Pail, T. Gruber, and X. Oikonomidou, "The Combined Global Gravity Field Model XGM2019e," Journal of geodesy, vol. 94, no. 7, article no. 66, 2020.

[19] Y. Wu, X. He, Z. Luo, and H. Shi, "An Assessment of Recently Released High-Degree Global Geopotential Models Based on Heterogeneous Geodetic and Ocean Data," Frontiers in Earth Science, vol. 9, article no. 749611, 2021.

[20] E. Nicacio, R. Dalazoana, and S. De Freitas, "Evaluation of the Ultra-High Resolution Global Geopotential Model SGG-UGM-1 in the Brazilian Southern Region," in VII Simpósio Brasileiro de Ciências Geodésicas e Tecnologias da Geoinformação, pp. 609-618, 2018.

[21] Google, "Google Earth," https://satellites.pro/Google/Lebanon_map, accessed in 2023.

[22] NASA, "Earth Data," https://www.earthdata.nasa.gov/, accessed in 2023.

[23] M. M. Gazizovich and M. Nasrullah, "Estimating Coordinates Transformation Parameters from Global to Local Coordinates Systems in Lebanese Republic Based on Zonal Division," International Journal of Engineering, vol. 38, no. 4, pp. 796-806, 2025.

[24] O. C. Ibe, Fundamentals of Applied Probability and Random Processes, 2nd ed., Academic Press, 2014.

[25] A. J. Hayter, Probability and Statistics for Engineers and Scientists, 4th ed., Brooks/Cole: Cengage Learning, 2012.

[26] T. G. Farr, P. A. Rosen, E. Caro, R. Crippen, R. Duren, S. Hensley, et al., "The Shuttle Radar Topography Mission," Reviews of geophysics, vol. 45, no. 2, 2007.

[27] E. Uuemaa, S. Ahi, B. Montibeller, M. Muru, and A. Kmoch, "Vertical Accuracy of Freely Available Global Digital Elevation Models (ASTER, AW3D30, MERIT, TanDEM-X, SRTM, and NASADEM)," Remote Sensing, vol. 12, no. 21, article no. 3482, 2020.

[28] D. C. Montgomery and G. C. Runger, Applied Statistics and Probability for Engineers, 7th ed., Hoboken, NJ: Wiley, 2018.

Copyright© by the authors. Licensee TAETI, Taiwan. This article is an open-access article distributed under the terms and conditions of the Creative Commons Attribution (CC BY-NC) license (https://creativecommons.org/licenses/by-nc/4.0/).